Low-noise transition edge sensor (TES) for SAFARI instrument on SPICA

P. Khosropanah[a*], B. Dirks[a], M. Parra-Borderías[b], M. Ridder[a], R. Hijmering[a], J. van der Kuur[a], L. Gottardi[a], M. Bruijn[a], M. Popescu[a], J. R. Gao[ac], H. Hoevers[a]

[a]SRON Netherlands Institute for Space Research, Utrecht/Groningen, the Netherlands

[b]Instituto de Ciencia de Materiales de Aragón, CSIC-Universidad de Zaragoza, Departamento de FÌsica de la Materia Condensada

[c]Kavli Institute of NanoScience, Delft University of Technology, Delft, the Netherlands

ABSTRACT

Transition edge sensor (TES) is the selected detector for the SAFARI FIR imaging spectrometer (focal plane arrays covering a wavelength range from 30 to 210 μm) on the Japanese SPICA telescope. Since the telescope is cooled to <7 K, the instrument sensitivity is limited by the detector noise. Therefore among all the requirements, a crucial one is the sensitivity, which should reach an NEP (Noise Equivalent Power) as low as 3×10^{-19} W/Hz^0.5 for a base temperature of >50 mK. Also the time constant should be below 8 ms.

We fabricated and characterized low thermal conductance transition edge sensors (TES) for SAFARI instrument on SPICA. The device is based on a superconducting Ti/Au bilayer deposited on suspended SiN membrane. The critical temperature of the device is 155 mK. The low thermal conductance is realized by using narrow SiN ring-like supporting structures. All measurements were performed having the device in a light-tight box, which to a great extent eliminates the loading of the background radiation. We measured the current-voltage (IV) characteristics of the device in different bath temperatures and determine the thermal conductance (G) to be equal to 1.66 pW/K. This value corresponds to a noise equivalent power (NEP) of 1×10^{-18} W/√Hz. The current noise and complex impedance is also measured at different bias points at 25 mK bath temperature. The measured electrical (dark) NEP is 2×10^{-18} W/√Hz, which is about a factor of 2 higher than what we expect from the thermal conductance that comes out of the IV curves. Despite using a light-tight box, the photon noise might still be the source of this excess noise. We also measured the complex impedance of the same device at several bias points. Fitting a simple first order thermal-electrical model to the measured data, we find an effective time constant of about 65 μs and a thermal capacity of 3-4 fJ/K in the middle of the transition.

Keywords: Transition-edge sensor, TES, far infra-red spectrometer, submm spectrometer, SiN membrane.

*P.Khosropanah@sron.nl; phone +31 88777 5678; fax +31 88777 5601; sron.nl

Millimeter, Submillimeter, and Far-Infrared Detectors and Instrumentation for Astronomy V,
edited by Wayne S. Holland, Jonas Zmuidzinas, Proc. of SPIE Vol. 7741, 77410L

1. INTRODUCTION

SPICA[1] is a Japanese-led mission to fly a 3.5 m diameter IR telescope with cryogenically cooled (about 5 K) mirror. Cooling the optics reduces the background radiation that limits the sensitivity of ambient temperature FIR space telescopes. The loading is then dominated by astrophysical background sources.

The SAFARI[2] instrument is one of three instruments on SPICA. It is an imaging Fourier Transform Spectrometer (FTS) with three bands covering the wavelength ranges: 35-60 μm, 60-110 μm, and 110-210 μm. The loading in these bands is estimated to be dominated by emission from the Zodiacal light at a level of 0.3-1 fW.[2] This gives a photon noise equivalent power (NEP) at the detectors of $1\text{-}3\times10^{-18}$ W/√Hz. Therefore, we require detectors with electrical NEPs at least 3 times lower than the photon noise limit, i.e. $\leq 3\times10^{-19}$ W/√Hz. This is about 2 orders of magnitude higher sensitivity than what is required for detectors on a ground based telescope and impose a great challenge on the detector technology. The requirement for the response time of the detectors for SAFARI is set to $\tau \leq 8$ ms by the maximum scanning speed of the FTS mechanism and the downlink bandwidth.

Transition edge sensor (TES) is the selected detector technology for the SAFARI. Silicon nitride suspended bolometers (although not for TESs) were originally developed for ground-based mm-wave observations and have been used in a large number of ground-based and sub-orbital experiments.[3-6] Silicon nitride suspended structures were used in the Herschel-SPIRE[7] and the Planck-HFI.[8] All of the detectors in these instruments use bolometer chips that are bonded to the silicon nitride membranes in a hybrid process.[9,10] More recently, a number of groups have developed bolometers incorporating silicon nitride thermal isolation combined with TES bolometers (see Ref. 11 and references therein). Such detectors together with SQUID multiplexed readout are currently used in a number of ground-based and balloon-borne instruments such as SCUBA2, APEX-SZ, CLOVER, EBEX and SPIDER.

In collaboration with a European TES team, SRON is developing low thermal conductance TES bolometers for SPICA. These devices are based on Ti/Au bilayer as sensitive element on suspended silicon nitride membranes.

Previously we reported measurements of a single pixel TES using long straight legs.[12] Also the optical test of a similar TES integrated with an absorber was reported.[13] In order to achieve very low thermal conductance we needed to use 4 very long legs of about 1800 μm. This makes the devices size rather large and therefore not suitable for making arrays with required pitch size for the SAFARI. In the current design the TES is supported by ring structures that allows for making low-G device in much smaller space. Besides, an array of 5×5 of these devices was fabricated with required SAFARI short wavelength pitch size, that is 480 μm.

Here we present the details of the detector design and electrical (dark) characterization, including IVs, noise, complex impedance data and the analysis.

2. TES DEVICE

The device under test is based on Ti/Au (16/60 nm) bilayer, deposited on 1 μm thick suspended SiN membrane. The TES size is 50×50 μm^2 and the critical temperature (T_c) is 155 mK. In order to be able to test this device optically (not reported here), we have an absorber close to the TES which is a 55×55 μm^2 Ta with thickness of 8 nm. The absorber and the TES are sitting on a $120\times120\times1$ μm^3 SiN membrane.

Fig. 1 shows a picture of this device. The SiN supporting structure consists of 12 rings, each 4 μm wide that are place in 10 μm apart. Each ring is connected to the adjacent rings via 4 radial piece of SiN. The electrical contact to the bolometer is realized via 90 nm thick, 3 μm wide Nb wiring on the top of SiN structure. Our design target was a thermal conductance (G) of about 1.26 fW/K that corresponds to an NEP of 1×10^{-18} W/√Hz, taking only the phonon noise into account.

This device is a pixel in an array of 5×5 with a pitch size of 480 μm, which is required by the SAFARI short wavelength focal plane array. Realizing this bolometer using four straight leg requires over 1000 μm long legs which obviously does not fit into pitch size requirement. *Tc* of 10 devices on such array were measured and show less than 5% variation.

This devices was clearly not designed to meet the outmost sensitivity requirement for SAFARI. It is an intermediate step to demonstrate the technology of the TES with supporting ring-like structure and at the same time investigate the scalability by fabricating an small array.

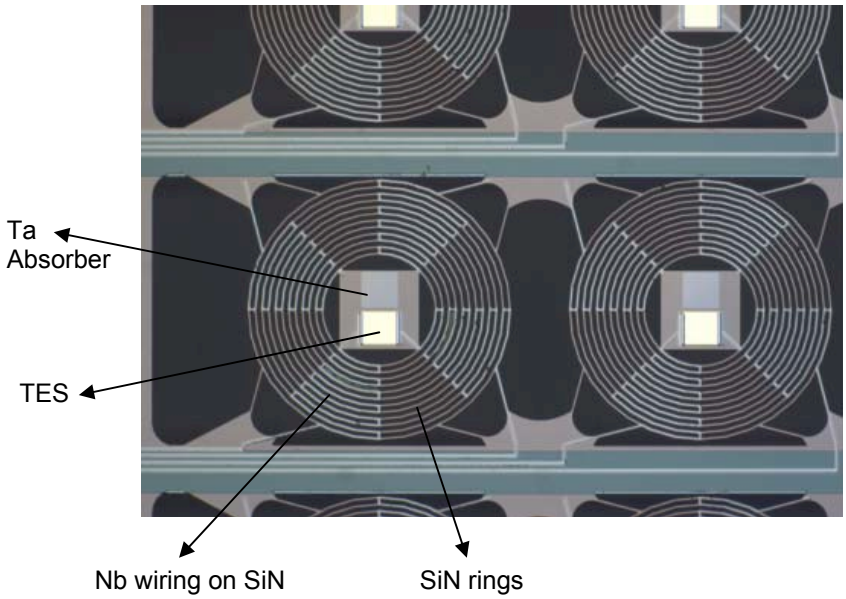

Figure 1. The TES device as part of 5×5 array.

3. CURRENT-VOLATGE CHARACTERISTICS

The sample is tested using a Kelvinox dilution fridge that is able to cool down the device to 16 mK. The detector is mounted in a light tight box, which is designed to minimize the background loading due to possible stray light. The electrical wiring into this box goes through a meander path that is filled with Stycast mixed with SiC grains. We estimate the power leakage to the box to be below 0.2 fW which is relatively low compared to our power levels in the IV measurement (see Fig. 4). Therefore, we are confident that the outcome of our IV test is quite dark and therefore reliable.

Fig. 2 shows a schematic diagram of the measurement circuit. The biasing is done by using a current source in parallel with 5 mΩ shunt resistance (*Rshunt*) that simulates a voltage bias. The total bias resistance is then the *Rloud* in parallel with the *Rshunt*, giving a value less than 5 mΩ, which provides a solid voltage bias for the points where data were taken. In addition, there is a parasitic resistance, in series with the TES, which is denoted as *Rseries* and is about 0.2 mΩ. The TES current is read out using a SQUID with a closed flux locked loop.

Fig. 3 shows a set of measured IV curves at bath temperatures varying from 25 to 150 mK.. The dc power in the transition at each bath temperature is almost constant. Fig. 4 shows the power level as a function of bath temperature.

The heat flow equation for a TES can be written as:

$$P = K(T_C - T_{bath})^n \tag{1}$$

where P is the bias power applied to TES; K a constant that depends on the geometry and material properties of the supporting legs; T_C the critical temperature of the bilayer; and T_{bath} the bath temperature. In Eq. (1) all are known except for n and K, We can fit Eq. (1) to the measured data to find both values. For this device the best fit was obtain using n = 3.4 and K = 0.44 pW/K^n.

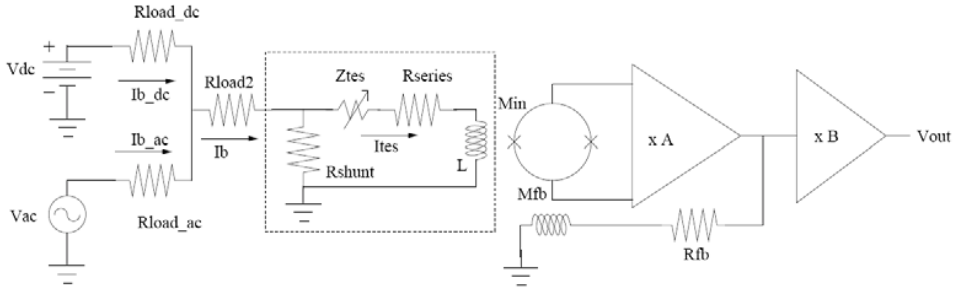

Figure 2. Schematic picture of the TES measurement circuit. In case of IV and noise measurement there is no ac bias source. In complex impedance measurement a 10 kΩ resistor followed by an amplifier is used as a wide band noise source and sits at *Vac* in the circuit.

The fundamental intrinsic phonon noise in TES can be written as:[14]

$$NEP = \sqrt{\gamma 4 k_B T^2 G}\ . \tag{2}$$

Here γ is a number between 0.5 and 1 that accounts for temperature gradient along the supporting legs. *kB* is the Boltzmann's constant, *T* is the temperature of the TES and *G* is the thermal conductance between the TES and the substrate which can be written as:

$$G = nKTc^{n-1}\ . \tag{3}$$

Inserting the values from the fit in Fig. 4 gives a *G* of 1.66 fW/K, which in turn results in an NEP of 1×10^{-18} W/√Hz using Eq. (2).

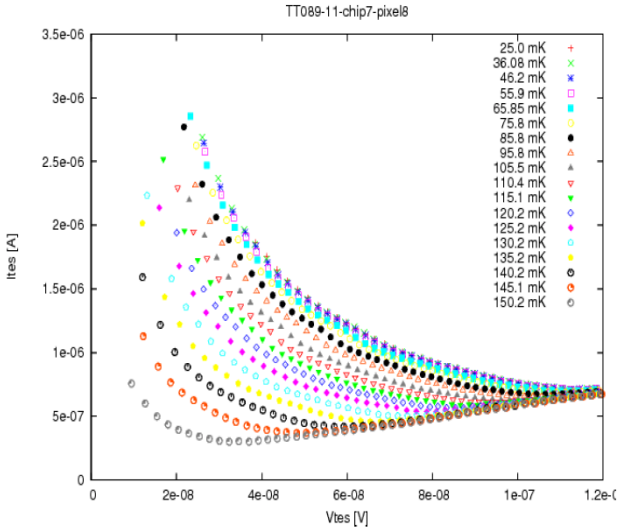

Figure 3. IV curves at different bath temperature. *Ites* is the current through the TES and *Vtes* is the voltage across the device.

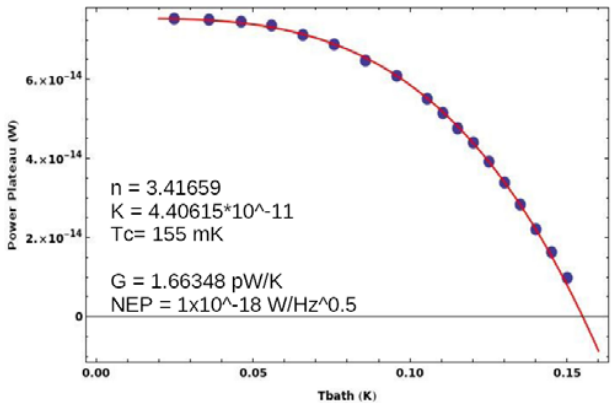

Figure 4. Power plateaus in the transition as a function of bath temperature.

4. NOISE MEASUREMENT

Fig. 5 shows the measured current noise spectra at several bias points in the transition at 25 mK bath temperature. The data has a frequency resolution of 2 Hz. Multiplying the current noise level at low frequency (for instance at 10 Hz) with the bias voltage yields a dark NEP, which is about $2\text{x}10^{-18}$ W/√Hz. This means that the measured dark NEP is about a factor of 2 higher than what we expect from the measured *G*. We also see that there is a hump in the noise spectra above 1 kHz that grows as we move down in the transition. The reason for this is currently under study. This can be due to an excess noise often found in TES and can also be due to photon noise by remaining stray light in spite of using the light tight box.

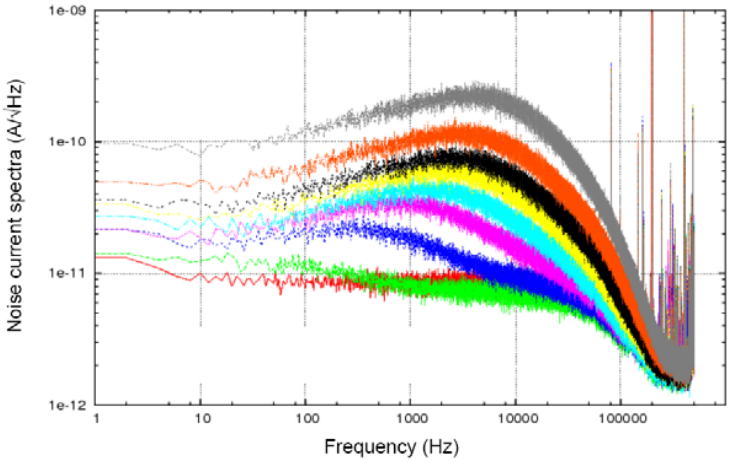

Figure 5. Noise current spectra measured in the transition that corresponds to NEP= 2×10^{-18} W/√Hz. The red curve is high in transition (close to normal state) and the gray curve is up in the transition (close to superconducting state).

5. COMPLEX IMPEDANCE MEASUREMENT

Fig. 2 shows the circuit that is used for measuring the complex impedance of the TES. Instead of the *Vac* we use a 10 kΩ resistance as a noise source. This noise is amplified and then added to the dc bias. Both the input noise signal and the output noise of the SQUID amplifier are recorded. The complex impedance of TES can be written as:

$$Z_{TES}(j\omega) = \frac{V_{AC}(j\omega)}{(R_{loadAC} + R_{load\,2}) \cdot I_{TES}(j\omega)} \cdot T(j\omega) - Z_{Th}(j\omega)\,. \tag{4}$$

where

$$Z_{Th}(j\omega) = R_{series} + R_{shunt} + j\omega L \,. \tag{5}$$

Here $T(j\omega)$ is the transfer function of the signal lines that is determined experimentally. In order to calculate the $Z_{TES}(j\omega)$ from Eq. (4) and (5) we need to find out $T(j\omega)$ and L. All other parameters are known. These two can be calculated by using two set of equations for superconducting and normal state where Z_{TES} is known. At the superconducting state the $Z_{TES}(j\omega)$ is simply zero and at the normal state it is the normal resistance of the TES which is in our case equals 0.21 Ω. The L we get in this way is 0.5 μH.

Fig. 6 shows measured and fitted complex impedance curves at 4 different bias points at 25 mK bath temperature. In order to extract the TES parameters from the data we chose a simple, first order model that is described in great detail in Ref.11. In this model TES is seen as an isolated element with a certain heat capacity C that is connected to the bath with a low heat conductance G.

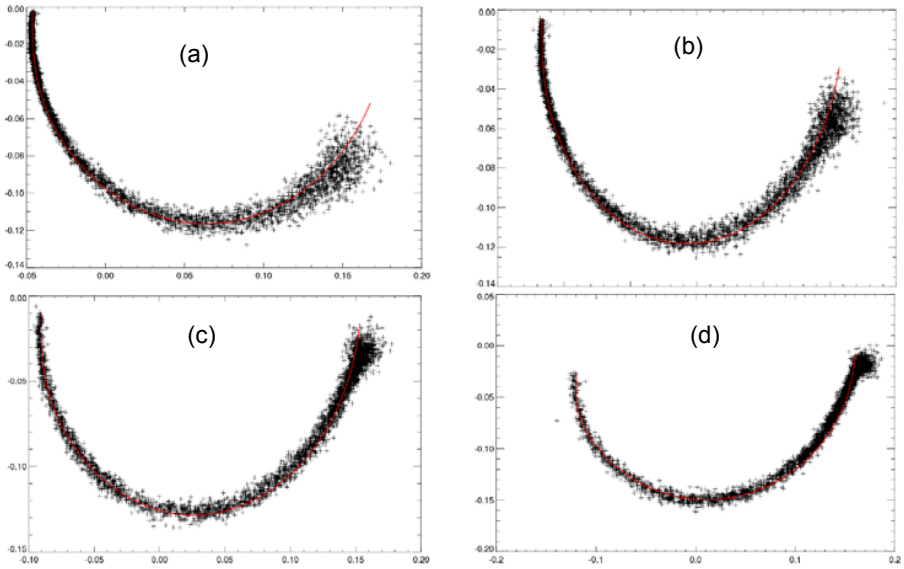

Fig. 6. Measured TES complex impedance (dots) and the fitted curves (red lines). The x-axis is the real part and the y-axes is the imaginary part in all curves. The measured impedance is shown at four different bias points: (a) high in the transition (close to normal state). (b) and (c) in middle of transition and (d) is low in transition (close to superconducting state).

As we can see in Fig. 6, the curves fit reasonably well to the measured data. In order to fully explain the device behavior more sophisticated models are needed that should take into account for dangling heat capacitances and perhaps distributed heat capacitance in the legs. On the other hand, we noticed that the measured data are not far from model predictions and in first order the device can be reasonably explained by the simple model.

After having performed lengthy calculations using the electrical and thermal equations, the Z_{TES} can be written as:

$$Z_{TES} = Z_{\infty} + (Z_{\infty} - Z_0) \cdot \frac{1}{-1 + i\omega\tau_{eff}} \,. \tag{6}$$

where Z_0 and Z_∞ are the impedances at zero and at very high frequency, respectively. τ_{eff} is the effective time constant which is:

$$\tau_{eff} = \frac{\tau_0}{L_0 - 1} \,. \tag{7}$$

Here $\tau_0 = C/G$ is the intrinsic time constant and L_0 is defined as low frequency loop gain which is:

$$L_0 = \frac{P_0 \alpha}{G T_0}. \tag{8}$$

Here P_0 is the dc bias power and T_0 is the temperature of TES, which is close to T_C in the transition. α is the resistance dependence to the temperature at constant bias current and defined as:

$$\alpha = \frac{T_0}{R_0} \frac{\partial R}{\partial T}\bigg|_{I_0}. \tag{9}$$

In this model Z_0 and Z_∞ are written as:

$$Z_0 = R_0 \frac{1 + \beta + L_0}{1 - L_0}. \tag{10}$$

$$Z_\infty = R_0 (1 + \beta). \tag{11}$$

Here β is a measure of the resistance dependence of the current at constant temperature, which is defined as:

$$\beta = \frac{I_0}{R_0} \frac{\partial R}{\partial I}\bigg|_{T_0}. \tag{12}$$

By choosing the Z_0, Z_∞ and τ_{eff} at every bias point Eq. (6) is fitted to the measured data. Having Known Z_∞ and R_0 we derived β from Eq. (11) and using that in Eq. (10), L_0 will be known. Knowing the loop gain (L_0) and effective time constant (τ_{eff}), Eq. (7) gives us the intrinsic time constant (τ_0) and since the thermal conductance (G) is known from the IV measurement, we can estimate the thermal capacity (C) of the TES. Table 1 summarizes the outcome of this analysis for the TES in the middle of the transition.

Table 2. TES parameters from complex impedance measurement in the middle of the transition which is bias point number (c) in Fig. 6.

TES parameter	Value
G	1.66 pW/K
C	3 fJ/K
τ_0	2 ms
τ_{eff}	65 μs
L_0	31
R_0	210 mΩ
P_0	80 fW
α	100
β	1

6. SUMMARY AND CONCLUSIONS

We have fabricated and measured low thermal conductance array of TES devices as required for SPICA. We measured IV curves of a TES device at different bath temperatures from 25 to 155 mK while it is mounted in a light-tight box in order to minimize the background load. The dc bias power level is 78 fW at 25 mk. The thermal conductance extracted from the IV curves is 1.66 pW/K that corresponds to phonon noise NEP of 1×10^{-18} W/√Hz. Our noise measurement however shows a dark NEP of 2×10^{-18} W/√Hz. The source of excess noise is not clear at the moment.

This devices was clearly not designed to meet the outmost sensitivity requirement for SAFARI. It is to demonstrate the technology of the TES with supporting ring-like structure and at the same time investigate the scalability by going toward fabricating an small array. Increasing number of rings, narrowing the width of the legs and lowering the T_C of the device are the obvious ways of reducing the NEP further to meet the SAFARI specifications.

Our complex impedance data can be relatively well described by a simple, first order model. We derive a heat capacity of 3-4 fJ/K and an effective time constant of about 65 μs when the TES is in the middle of transition. These values are reasonably close to our designed values. The speed of the device is well below the specification for SPICA and can be further compromised by lowering the G to meet the sensitivity requirement.

The total heat capacitance of our device is dominated by that of silicon nitride membrane and expected to be about 30 fJ/K. This estimation is based on heat capacity measurements done on a suspended silicon nitride membrane with a size of 100×100×1 μm^3 at 250-800 mK.[15] The reason for seeing low heat capacity 3-4 fJ/K is not clear. More devices with different dimensions should be measured to clarify this point. For further study of low thermal conductance TES and discussion on SiN heat capacity see Ref.16 and 17. This work is partly supported by ESA under TRP program contract no. 22359/09/NL/CP, TES Spectrometer.

REFERENCES

1. H. Kaneda, T. Nakagawa, T. Onaka, T. Matsumoto, H. Murakami, K. Enya, H. Kataza, H. Matsuhara, and Y. Y. Yui, "Development of space infrared telescope for the SPICA mission," in Optical, Infrared, and Millimeter Space Telescopes. Edited by Mather, John C. Proceedings of the SPIE, Volume 5487, pp. 991-1000 (2004).
2. B. Swinyard, "Esi: the far-infrared instrument for the spica mission," Space Telescopes and Instrumentation I: Optical, Infrared, and Millimeter 6265(1), p. 62650L, SPIE, 2006.
3. B. Benson, S. Church, P. Ade, J. Bock, K. Ganga, C. Henson, and K. Thompson, "Measurements of Sunyaev-Zel'dovich effect scaling relations for clusters of galaxies," Astrophysical Journal 617, pp. 829–846, DEC 20 2004.
4. G. W. Wilson, J. E. Austermann, T. A. Perera, K. S. Scott, P. A. R. Ade, J. J. Bock, J. Glenn, S. R. Golwala, S. Kim, Y. Kang, D. Lydon, P. D. Mauskopf, C. R. Predmore, C. M. Roberts, K. Souccar, and M. S. Yun, "The AzTEC mm-wavelength camera," Monthly Notices of the Royal Astronomical Society 386, pp. 807–818, MAY 11 2008.
5. F. Piacentini, P. Ade, R. Bhatia, J. Bock, A. Boscaleri, P. Cardoni, B. Crill, P. de Bernardis, H. Del Castillo, G. De Troia, P. Farese, M. Giacometti, E. Hivon, V. Hristov, A. Iacoangeli, A. Lange, S. Masi, P. Mauskopf, L. Miglio, C. Netterfield, P. Palangio, E. Pascale, A. Raccanelli, S. Rao, G. Romeo, J. Ruhl, and F. Scaramuzzi, "The BOOMERANG North America instrument: A balloon-borne bolometric radiometer optimized for measurements of cosmic background radiation anisotropies from 0.degrees 3 to 4 degrees," Astrophysical Journal Supplement Series 138, pp. 315–336, FEB 2002.
6. S. Masi, P. A. R. Ade, J. J. Bock, J. R. Bond, J. Borrill, A. Boscaleri, P. Cabella, C. R. Contaldi, B. P. Crill, P. de Bernardis, G. De Gasperis, A. de Oliveira-Costa, G. De Troia, G. Di Stefano, P. Ehlers, E. Hivon, V. Hristov, A. Iacoangeli, A. H. Jaffe, W. C. Jones, T. S. Kisner, A. E. Lange, C. J. MacTavish, C. M. Bettolo, P. Mason, P. D. Mauskopf, T. E. Montroy, F. Nati, L. Nati, P. Natoli, C. B. Netterfield, E. Pascale, F. Piacentini, D. Pogosyan, G. Polenta, S. Prunet, S. Ricciardi, G. Romeo, J. E. Ruhl, P. Santini, M. Tegmark, E. Torbet, M. Veneziani, and N. Vittorio, "Instrument, method, brightness, and polarization maps from the 2003 flight of BOOMERanG," Astronomy & Astrophysics 458, pp. 687–716, NOV 2006
7. M. Griffin, A. Abergel, P. Ade, P. Andr´e, J.-P. Baluteau, J. Bock, A. Franceschini, W. Gear, J. Glenn, D. Griffin, K. King, E. Lellouch, D. Naylor, G. Olofsson, I. Perez-Fournon, M. Rowan-Robinson, P. Saraceno, E. Sawyer, A. Smith, B. Swinyard, L. Vigroux, and G. Wright, "Herschel-SPIRE: design, performance, and scientific capabilities," in Space Telescopes and Instrumentation I: Optical, Infrared, and Millimeter. Proceedings of the SPIE, Volume 6265, pp. 62650A (2006).
8. J.-M. Lamarre, J. L. Puget, M. Piat, P. A. R. Ade, A. E. Lange, A. Benoit, P. De Bernardis, F. R. Bouchet, J. J. Bock, F. X. Desert, R. J. Emery, M. Giard, B. Maffei, J. A. Murphy, J.-P. Torre, R. Bhatia, R. V. Sudiwala, and V. Yourchenko, "Planck high-frequency instrument," in IR Space Telescopes and Instruments. Edited by John C. Mather . Proceedings of the SPIE, Volume 4850, pp. 730-739 (2003).
9. A. Turner, J. Bock, J. Beeman, J. Glenn, P. Hargrave, V. Hristov, H. Nguyen, F. Rahman, S. Sethuraman, and A. Woodcraft, "Silicon nitride micromesh bolometer array for submillimeter astrophysics," Applied Optics 40, pp. 4921–4932, OCT 1 2001.

10. P. D. Mauskopf, J. J. Bock, H. del Castillo, W. L. Holzapfel, and A. E. Lange, “Composite infrared bolometers with Si3N4 micromesh absorbers,” Applied Optics 36, pp. 765–771, Feb. 1997.
11. K. Irwin and G. Hilton, “Transition-edge sensors”, Cryogenic Particle Detection 99, pp. 63–149, 2005.
12. P. Khosropanah, B. Dirks, J. van der Kuur, M. Ridder, M. Bruijn, M. Popescu, H. Hoevers, J. R. Gao, D. Morozov, and P. Mauskopf, "Low Thermal Conductance Transition Edge Sensor (TES) for SPICA", AIP Conf. Proc. 1185, 42 (2009), DOI:10.1063/1.3292369
13. D. Morozov, P. D. Mauskopf, P. Ade, M. Bruijn, P. A. J. de Korte, H. Hoevers, M. Ridder, P. Khosropanah, B. Dirks, and J.-R. Gao, "Ultrasensitive TES bolometers for space based FIR astronomy", AIP Conf. Proc. 1185, 48 (2009), DOI:10.1063/1.3292385
14. J. Mather, “Bolometer noise: nonequilibrium theory”, Appl. Opt. 21, 1125-1129 (1982).
15. K. Rostem, D.M. Glowacka, D. J. Goldie, and S. Withington, “Thermal conductance measurements for the development of ultra low-noise transition-edge sensors with a new method for measuring the noise equivalent power”, Proc. SPIE 7020, 70200L (2008).
16. M. Kenyon, P. K. Day, C. M. Bradford, J. J. Bock, and H. G. Leduc, "Progress on background-limited membrane-isolated TES bolometers for far-IR/submillimeter spectroscopy", Proc. SPIE 6275, 627508 (2006), DOI:10.1117/12.672036
17. M. Kenyon, P. K. Day, C. M. Bradford, J. J. Bock, and H. G. Leduc, "Ultra-sensitive transition-edge sensors (TESs) for far-IR/submm space-borne spectroscopy", AIP Conf. Proc. 1185, 56 (2009), DOI:10.1063/1.3292406